CHAPTER – 3

Observation of Unusual Griffith's Phase behavior and dielectric properties in Quadruple perovskite oxide CaCu3Mn4O12 (CCMO) Synthesized through Chemical Route

3.1 Introduction

$CaCu_3Mn_4O_{12}$ (CCMO) complex perovskite has much-attracted the attention of the researchers. (Chenavas et al. 1975) The crystal structure of $CaCu_3Mn_4O_{12}$ has John – teller distortion take place is due to the presence of copper ($Cu^{+2}d^9$ t_{2g}^6 and eg^3) or the presence of transition metal cation (Mn^{+3} oxidation state d^4 configuration t_2g^3andeg^1).(Deisenhofer et al. 2005)CCMO ceramic is a type of Perovskite oxide that has general formula is $AA'BO_3$ type where A and A'exists at the corner and B exists in the body-centered and oxygen occupied at the face of the cubic lattice respectively(Tararam et al. 2011). It has very much attracted considerable attention to structural and magnetic analysis. $CaCu_3Mn_4O_{12}$ is also the same analogous crystal structure $CaCu_3Ti_4O_{12}$ but magnetic properties have large differences that occur in CCMO Griffith's phase behavior but in CCTO not explain the existence of this type of disorder in previous.(Zheng et al. 2012),(Nurulhuda et al. 2017),(Liu et al. 2014 p. 9) In previously reported Griffith's phase behavior showing Perovskite (Bhoi et al. 2013; Deisenhofer et al. 2005), or anti peroskites(Lin et al. 2015) oxide explain to Griffith's phase through doping the of transition metals.

In this work, $CaCu_3Mn_4O_{12}$ ceramic was synthesized through the chemical route. The chemical route is more helpful for reaching chemical formula at the ionic level. In this chemical method, all-metal nitrates were taken in a stoichiometric amount to keep away avoiding the handling problem of chemicals (carbonate form such as metal carbonate form) and got the phase formation of CCMO ceramic. (Chenavas et al. 1975)It was observed that in CCMO ceramic a unique behavior of magnetic susceptibility disorder, the magnetic susceptibility (χ) of ferromagnetic materials can be described by Curie-Weiss (CW) law, and namely $1/\chi$ (T) is linearly dependent on temperature. When the temperature is well above T_C Curie-Weiss (CW) law has been

studied extensively demonstrated by either an upturn or a downward deviation from the linear temperature dependence of 1/χ (T) upon cooling. It has been well detected extensively a common downward deviation on 1/χ (T) in many magnetic materials, here the result was not very common that is where short-range (SR) FM clusters were found to be upon cooling and lastly developed long-range (LR) ordered below T_C. These types of dissimilarities are relatively few studies on the upturn deviation on 1/χ (T) above T_C, this behavior is known as Griffith's phase. (Bhoi et al. 2013) The unusual critical behaviors and the deviations of the magnetic susceptibility from the CW law have attracted much research interest clearly, but it is unknown whether and how the two issues are related. (Chenavas et al. 1975)

3.2. EXPERIMENTAL SECTION

Synthesis of material.

For the preparation of $CaCu_3Mn_4O_{12}$ (CCMO) ceramic, Chemical method was follow in which mixing of all-metal nitrate $Ca(NO_3)_2.4H_2O$ 98% Merck, India), $Cu(NO_3)_2.6H2O$ Pure 99% Merck, India, $C_4H_4MnO_4.H_2O$ (Aldrich 99 % Pure), All metal- nitrates were mixed in distilled water used as solvent in stoichiometric amounts and also used calculated amount of citric acid used as chelating agent (Citric acid $C_6H_8O_7$,99.5%, Emparta, India) equivalent to metal ions were dissolved in distilled water and mixed with the solution. Which was more suitable for reaching to purity as compared to sol gel technique in which impurity highly recorded of metal oxides besides CCMO peak through XRD pattern. The Calcium nitrate tetra hydrates, Copper nitrate hex hydrates, and Manganese citrate, Follow-on of these mixtures were magnetically stirred on a plate and slowly increased the temperature up to 70°C to 80°C, and maintain to this temperature for 12 to 15 hours to remove excess water and

accelerate to the polyaesterification. The light blue and sticky gels were formed of CCMO ceramic. The remaining quantity was dehydrated at 150℃ to 200℃ in hot air oven to fully evaporate water $CaCu_3Mn_4O_{12}$ (CCMO) was found as a black, well-crystallized powder form. The dry powder was ground into a fine powder using a mortar and pestle and calcined at 600℃ for 6 h in a muffle furnace follow on pelletization. Cylindrical pellets (12.9 mm x 0.90 mm) were prepared using with polyvinyl alcohol (PVA 2 wt. %) used as the binder with calcined powder was preparing by hydraulic press applying pressure of 4.5 to 5 tons for 1 min. This binder was burnt out at 450 °C for 2 h. The pellet was sintered in the high-temperature furnace at relatively low-temperature 800℃ for 6 h.

3.3. Results and discussion

Thermogravimetric Analysis (TGA)

Figure 3.1displays TGA plots of precursor powder of CCMO ceramic to study the ideal temperature for the decomposition of precursor dry powder. It indicates from the graph there are two steps of weight loss with the increasing temperature reaching up to 1000℃. The first weight loss was observed at around 475 ℃ to 625 ℃.(de Oliveira et al. 2016) The second weight loss started around 675 ℃ to 910 ℃ which indicates that the phase formation of CCMO ceramic. (Jaiswar and Mandal 2017),(de Oliveira et al. 2016) The $CaCu_3Mn_4O_{12}$ (CCMO) powder has been studied by with a heating rate of 10 °C min^{-1} from room temperature (RT) to 1000 °C in an inert air,(de Oliveira et al. 2016).

$Mn(NO_3)_2(aq) + 2C_2H_5NO_2(aq) + 2NH_4NO_3 + O_2 \rightarrow MnO_2(S) + 2N_2(g) + 4CO_2 + 5H_2O(g)$ **(Exothermic Reaction)**

$CaCO3 + CuO \rightarrow CaCu_3O_4 + CO_2(g) \uparrow$

$CaCu_3O_4 + 4MnO_2 \rightarrow CaCu_3Mn_4O_{12}$ ..... PRODUCT (1)

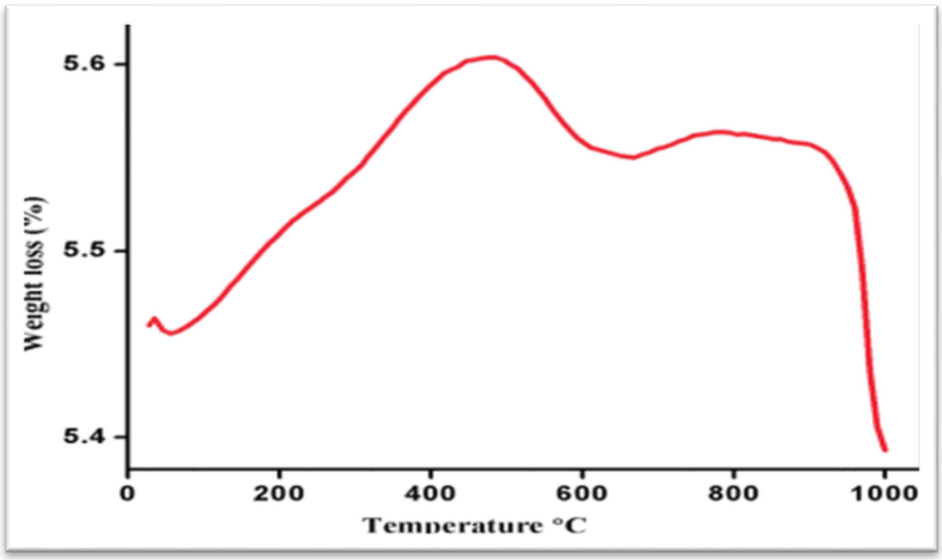

Figure 3.1. shows a TGA graph of $CaCu_3Mn_4O_{12}$ as- prepared powder**.**

Fourier Transform- Infrared spectroscopy (FT-IR)

FT-IR spectra of CCMO calcined powder indicated by red color and sintered pellets represented by green colour is shown in Figure 3.2. The absorption peak appears at lower wavenumber 668, 580,527 and 507 $cm^{-1}$is associated with M-O (M= Mn or Cu) bonds. The peaks observed at 668 cm^{-1} due to M-O bonds appears in both the conditions. The absorption peak due to Mn-O-Mn bonds is obtained at 451 and 423 cm^{-1} in calcined and sintered materials, respectively. The Ca–O bonds are also observed at 423 cm^{-1}. The absorption bands occur in the range between 380 and 700cm^{-1} arises due to mixed vibrations of CuO_4 and MnO_6 groups predominant in the CCMO. (Singh et al. 2014) This was considered to be stiffening of the network and structural rearrangement, which lead to the perovskite phase.

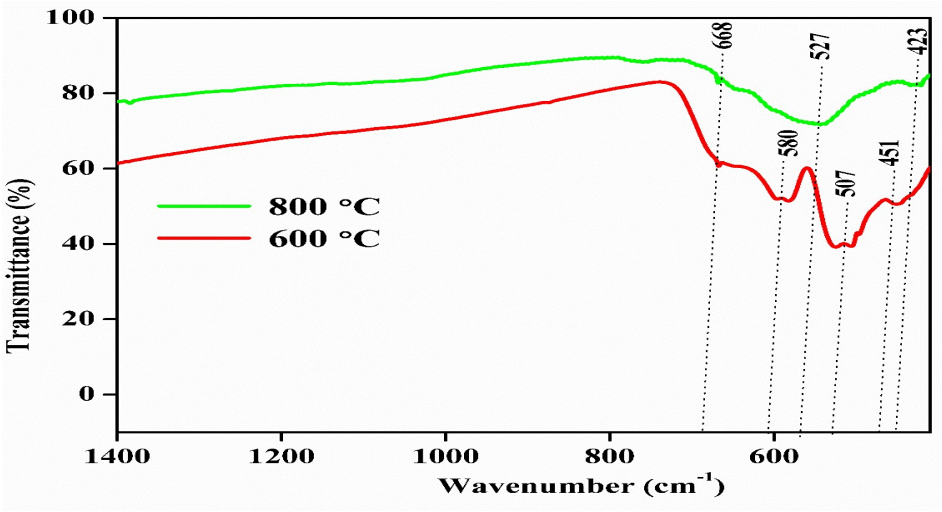

Figure 3.2. FTIR spectra of CCMO calcined powder at 600 °C for 6 h and sintered at 800 °C for 6 h different temperature.

X-ray diffraction (XRD) pattern

XRD pattern of CCMO ceramic calcined and sintered at 600℃, 800℃ for 6 h respectively is shown in Figure 3.3 which evidently emphasizes phase formation of CCMO with body-centered cubic structure. (Kim et al. 2012) Experimental data have been used to successfully confirm the CCMO ceramic and the only presence of minor CuO peak at grain-boundaries. Along with minor of which is with JCPDS card no. 80-1917. All the diffraction peaks of XRD patterns containing the planes (220), (220), (310), (321), (400), (332), (422), (510), (440) patterns which are correctly matched with the CCTO ceramic having CCTO (JCPDS 75-2188).(Thongbai et al. 2012) The lattice parameter and unit cell volume of CCMO ceramic was determined with the help of cell software. The presence of split peaks for the reflections 220, 422 in the sintered materials may be due to the existence of $CuK\alpha_2$ and $CuK\alpha_1$ radiations(Sharma et al. 2014). The average crystallite size (D) of CCMO ceramic was calculated by using the Debye Scherer's formula

$$D = \frac{k\lambda}{\beta \, Cos \ \theta}$$

…….. (2)

In the above equation (2) where k is the crystal shape coefficient (k = 0.89), λ is the wavelength (1.54 Å) of the X-ray, β is the full width at half maximum (FWHM) and θ is Braggs diffraction angle. The average value of crystallite size obtained for CCMO ceramic found to be 21.78 nm.

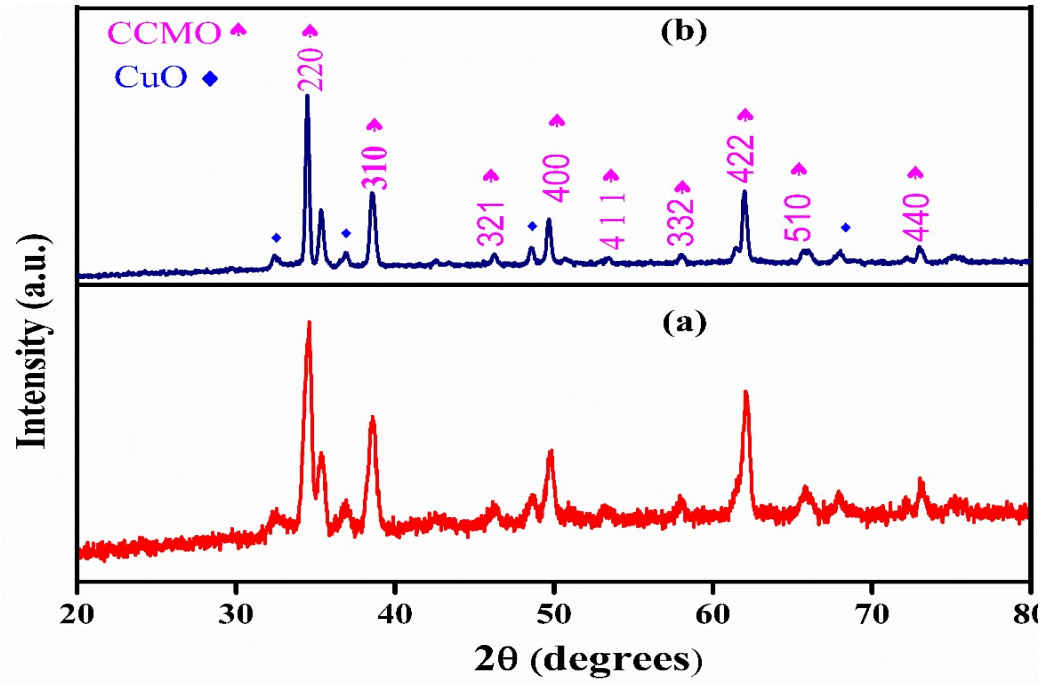

Figure 3.3. XRD pattern for $CaCu_3Mn_4O_{12}$ (CCMO) calcined at 600°C and sintered at 800°C 6 h respectively.

Raman studies

Figure 3.4 displays the Raman spectra of CCMO ceramic sintered at 850°C for 6 h. The highest intensity peak and lowest intensity peak position is observed at 785 cm^{-1} and 324 cm^{-1} which conforms the phase formation of CCMO ceramic. The lowest intensity peak observed at 324 cm^{-1} is evidently support the existence of CuO at the

grain boundary.(Kolev et al. 2002 p. 12) In Raman spectra which is displaying the graph, there are minor peaks observed lowest and highest intensity both, the peak position is at the 324 cm^{-1},376 cm^{-1},528 cm^{-1},599 cm^{-1},743 cm^{-1},785 cm^{-1},918 cm^{-1},991 cm^{-1}. In the above peak 324 cm^{-1} evidently shows and related to the Eg, 528 cm^{-1} and 599 cm^{-1} is associated with the A_1g symmetry octahedral MnO_6 rotation- like and peak observed at 599 cm^{-1} at Fg symmetry (Mn-O-Mn) anti stretching .the peak the highest intensity displaying at the position743 cm^{-1} could be to the first principle calculation, at 785 cm^{-1} this peak could be represented to the existence symmetrical stretching breathing of MnO . The low-intensity peak at the position was to be observed at the position 324 cm^{-1},376 cm^{-1} and 918 cm^{-1},991 cm^{-1} cm out of evidently two may be at first two not be expectable to the CCMO phase to the CCMO structure model, represent to the minor phase of CuO and MnO. In the CCMO ceramic peak observed at 324 cm^{-1} cm intensity represent to the grain boundary and supplementary peak, it was to be noted that also, 376 cm^{-1} and 599 cm^{-1} cm not found at the grain of CCMO. The peak intensity 376 cm^{-1} Raman spectral line-associated and justified the presence CuO in the grain boundary of CCMO ceramic and its active Raman mode A_2g which was already reported.

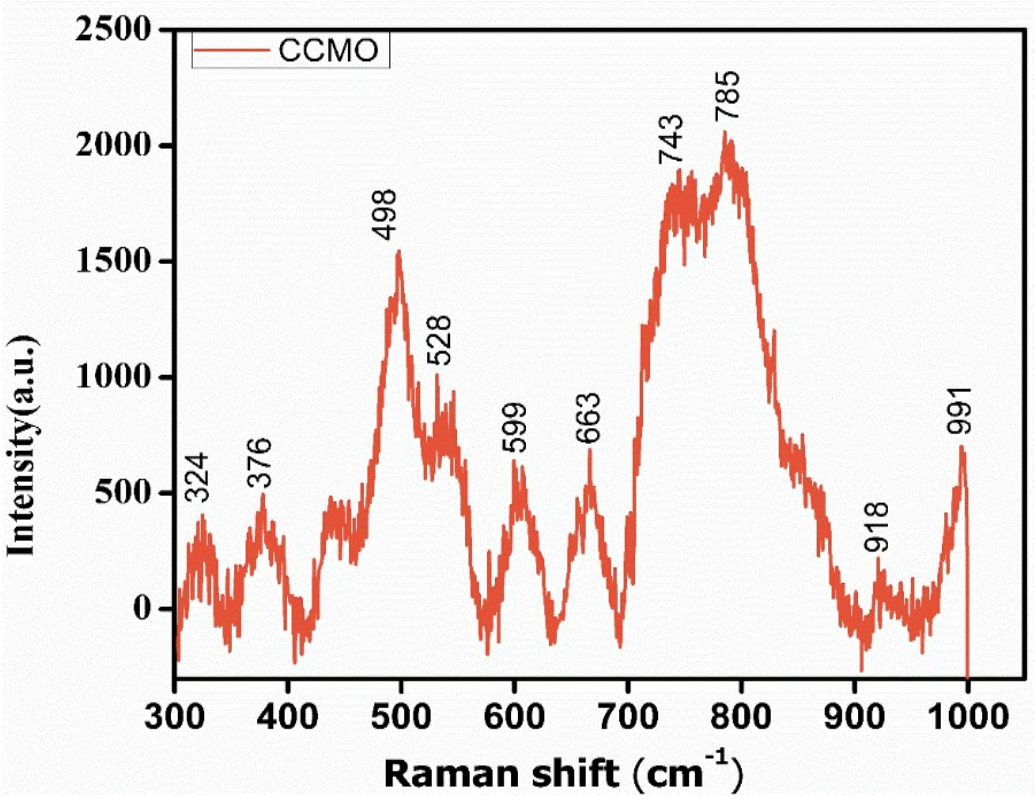

Figure 3.4. Raman spectra of $CaCu_3Mn_4O_{12}$ perovskite oxides sintered at 800°C for 6 h.

3.3.1 Microstructure studies

Field Emission -Scanning Electron Microscopic (FE-SEM) studies

The Morphology and microstructure of calcined powder and sintered pellet of CCMO at different temperatures were studied. The collection of some calcined powders of CCMO was detected in Figure 3.5 **(a)** shows the particles are improved in size by swelling the calcinations temperature which the lowest mean of particle sizes $CaCu_3Mn_4O_{12}$ are enlarged for sample calcined at 600°C for 6 h. The morphology of calcined powder of CCMO was initiating to the formation of a needle-like structure and occupying it at 800 °C for 6 h shown in Figure 3.5 b. (Nurulhuda et al. 2017) The grain size of the sintered CCMO compound was found to be 6.6×10^2 nm. In sintered pellet the

microstructure of CCMO morphology of grain size distribution is uniform, the grains are well developed compared to the sample 600 °C, particles are clearly visible the needle-like phase when sintered up to 800 °C. This uniformity of grain formation will promote the microstructural densification that will advantage in the conduction of electrical carriers and thus responsible for the improvement of conductivity. The measurements of the morphology of CCMO were successfully operated by using Image j software and find 6.6×10^2 nm by selecting 12 different grains for this operation. A comparison between micrograph Figure 3.5 (a) and (b) shown that the needles platelet-like particles were found after calcined to sintered 600℃ to 800 °C respectively. The FE-SEM micrograph shown the needle-like structure of CCMO sintered pellet at 800°C which creating out with equality of grain size distribution, fine particle size, and uniform development microstructure.(Nurulhuda et al. 2017),(Obrovac et al. 1998),(Lin et al. 2008)

Energy-Dispersive X-ray (EDX)

Figure 3.5 (C) indicates the chemical homogeneity of CCMO ceramic of atomic percentage was obtained by Energy-Dispersive X-ray (EDX) analysis of sintered pellet heated at 800°C for 6 h. The EDX spectra of the CCMO ceramic which confirms the presence of calcium, copper, manganese, and oxygen in the stoichiometric ratio. This indicates the elemental composition in which each element is shown by a specific colour , the distribution of the elements is homogeneous and heterogeneous in different areas. Their atomic percentages were detected to be 5.15, 16.79, 22.97 and 55.06 respectively. (Gautam et al. 2016a),(Singh et al. 2014)

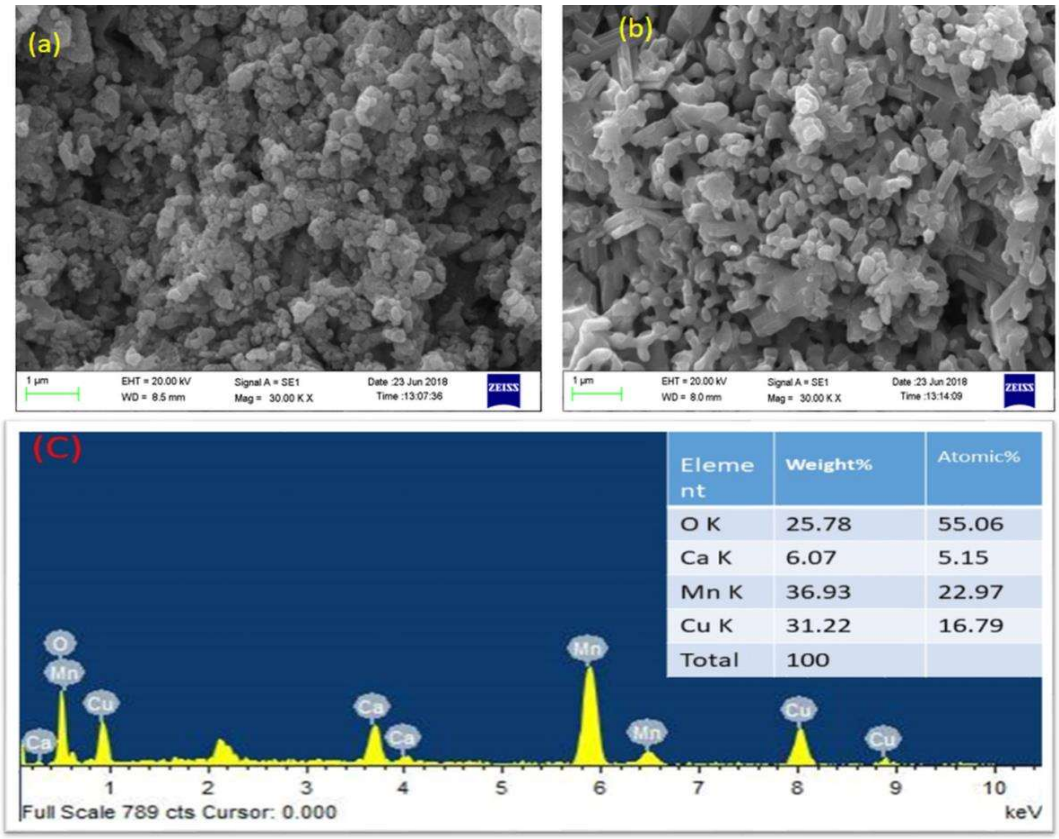

Figure 3.5 .(a) SEM micrographs of calcined at 600°C for 6 h **(b)** SEM micrographs of sintered at 800°C 6 h showing the needle-like structure and **(c)** shows the elemental analysis of CCMO ceramic.

High Resolution – Transmission Electron Microscopy (HR-TEM)

Figure 3.6 (a) and (b) indicate the Sintered CCMO 800℃ for 6 h. It is noted that the presence of the predominant cubical and spherical shape of the particle. It is observed the TEM that the range of particle by the plot of histogram 100-200 nm showing in Figure 3.7 (C) (Han et al. 2017).The particle size measured by TEM instrument it is noted that it shows the crystalline nature of the CCMO ceramic. Figure 5d indicates the

Selected Area Electron Diffraction (SAED) patterns show the parallel spots which confirm the presence normal peak of CCMO. (Deisenhofer et al. 2005) It is explained by the SAED pattern that the ring-like spots are indexed trough on the basis of basic of CCTO body-centered cubic (BCC) perovskite structure resemble CCTO ceramic which data also supported by XRD with JCPDS card no- 34-0097. These spots retain two different planes namely (2 1 1) and (1 1 0).It was also found through TEM the particle size of CCMO 100 to 200 nm which is proved that it has a nanocrystalline range and also supported by SEM.(Gautam et al. 2016a)

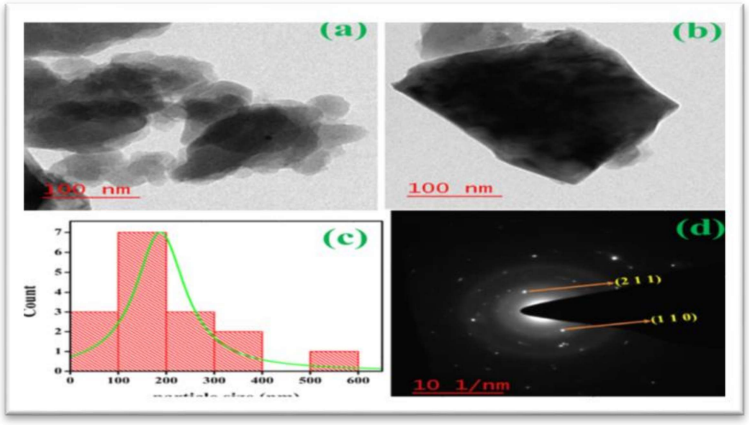

Figure 3.6 (a) Shows particle size of CCMO, **(b)** Shows cubical structure of CCMO, **(c)** Shows the histogram plot Of CCMO particle size and **(d)** Shows SEAD pattern of CCMO ceramic.

Atomic Force Microscopic studies (AFM)

Figure 3.7 (a) Shows 2-D AFM image of CCMO ceramic sintered at 800°C for 6 h reveals the presence of grains with bimodal structure separated by insulating grain boundaries. The average roughness (Ra) and root mean squire (RMS) was calculated by using Nova software for 3D image and found to be 45.797 and 54.275 nm, respectively on the covered area are 11×11 μm, where 1208 different point was used for calculation of mean value is shown in Fig. 6 (b). Fig. 6 (c)Shows histogram plots for particle size

which reveals that most of the roughness of particles was calculated in the range between 30±10 nm.(Tararam et al. 2011)

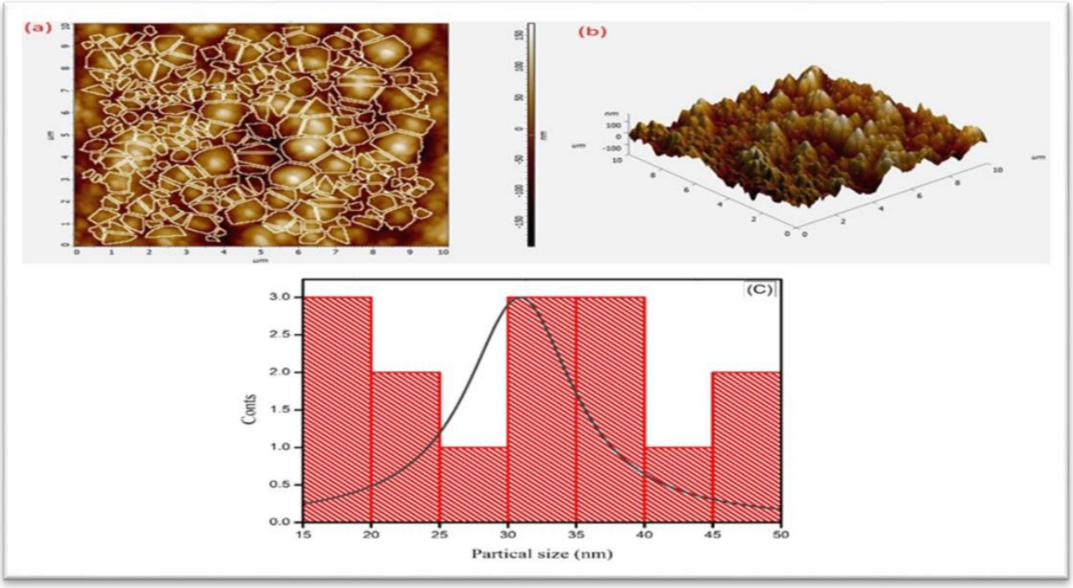

Figure 3.7. (a) AFM images of CCMO Ceramic sintered at 800°C for 6 h two-dimensional image showing grains and grain boundaries **(b)** Three-dimensional image of surface roughness of CCMO **(c)** Histogram of three-dimensional particle roughness.

X-Photoelectron Spectroscopy (XPS)

For the investigation of quantitative analysis of the elements was supported by XPS, In this spectra, it detected in CCMO ceramic which is the composition of polyvalent ion or different +2 in oxidation state sintered at 800°C for 6 hours. (Singh et al. 2014) It is showing in Figure 3.8 (a) to (d) the all the atom are present in different oxidation state in CCMO ceramic and showing them in the plot graph by binding energy versus intensity, Calcium(Ca in 2p), Copper (Cu in 2p), Manganese (Mn in 2p level) and Oxygen (O in 1s level) in the region. For analysis of this operation, there was taken compensation of low-energy electron charge of the C 1s peak at 284.6 eV was used to eliminate the effect of a positive charge on sample surfaces during XPS analysis. It is clear from the plot graph that in

by all spectra only matching peak with the Ca, Cu, Mn, O presented and evidenced the compositional pureness of the samples. Figure 3.10 (a) displays that the graph of intensity versus binding energy of Calcium (Ca^{+2}) +2 oxidation state in the CCMO ceramic and not only showing the binding energy (347 eV and 350.6 eV) of Calcium in 2p level but also from the shape and symmetry of the peak. The binding energy 934.54 eV and 954.23 eV by this is clear that Copper (Cu^{+2} in which Cu in 2p level)(Yamada et al. 2017), exist in +2 oxidation state which matches to Cu $^2p_{3/2}$ and Cu $^2p_{1/2}$ respectively displayed in Fig.7(b).(Singh et al. 2014)Fig. 7 (C) displays that Manganese exists in two different oxidation state Magneese (+iv) and Manganese present in (+iii) oxidation state (Mn^{+3}) on the basis binding energy versus intensity plotted graph 641.4 eV and 652.4 eV respectively.(Yang et al. 2015)[3],(Tang et al. 2014),(Verde et al. 2014)From the t Fig. 7 (d) the graph displays the binding energy peak of oxygen atom 929.7 eV and 931.6 eV lower and higher binding energy respectively. 929.7 eV peak shows are the slightly asymmetric type of 1s level(Jaiswar and Mandal 2017),(A. Molina-García and V. Rees 2016).

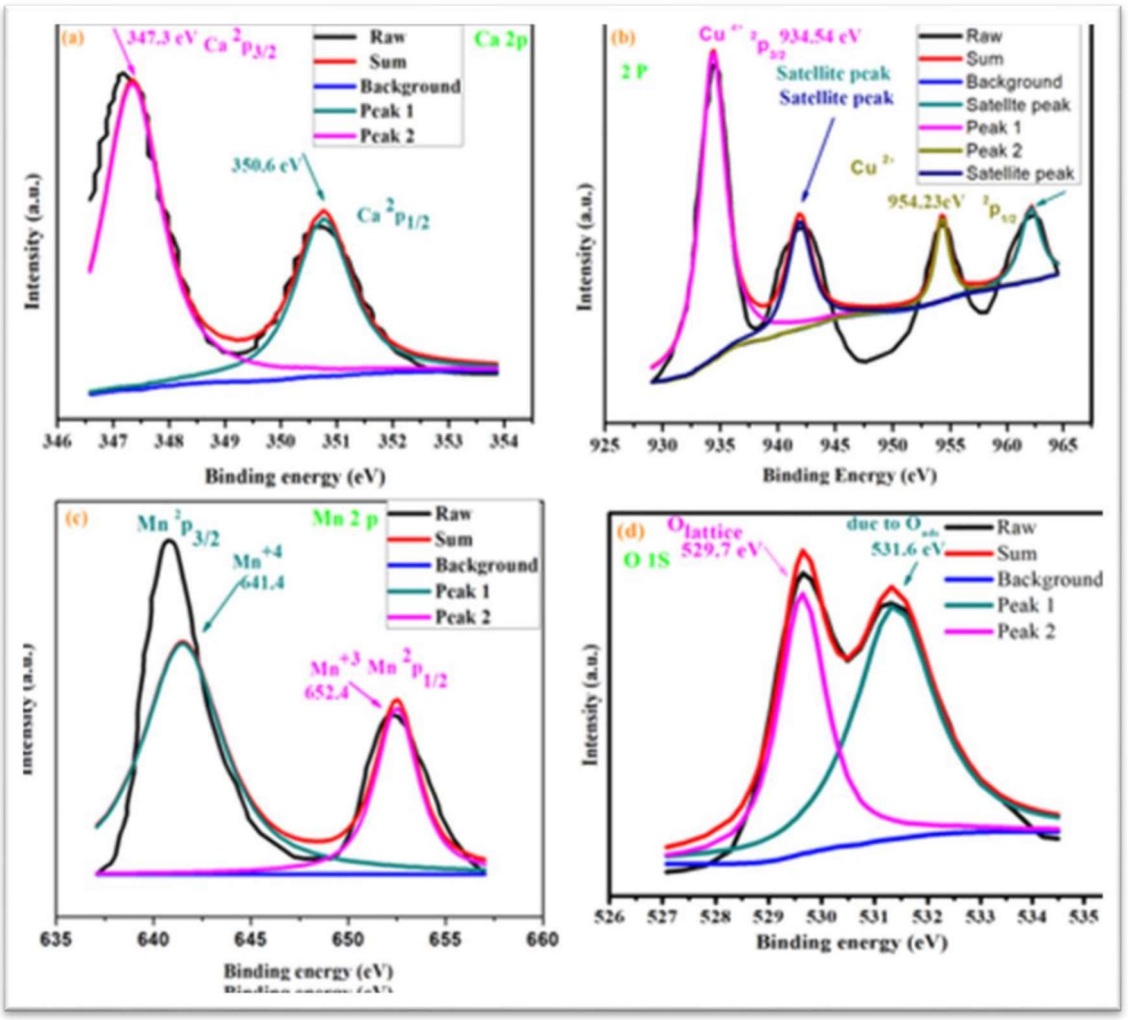

Figure 3.8. (a) XPS graph of Calcium oxidation state peak recorded at 347.3 eV and 350.7 eV.

(b) Shows the Copper oxidation state peak recorded at 934.54 eV and 954.23 eV.

(c) Shows the Manganese binding energy peak recorded at 641.4 eV and 652.4eV.

(d) Shows the Oxygen binding energy peak recorded at 529.7 and 531.6 eV.

3.3.2. Magnetic measurements

Figure 3.9 (a) displays to magnetization versus temperature. It is pointed out that from this plotted graph, the saturation of spontaneous ordering for the CCMO ceramic. It is also noted that there is a larger difference between ZFC and FC curve of the plotted

graph,(Thapa et al. n.d.)Which are suggesting that at very low temperature there were found the existence of a combination of ferromagnetic and antiferromagnetic checking slightly than separated long-range order. It is also noted that the existence of the magnetic of CCMO ceramic.(Jaiswar and Mandal 2017) It was observed the ZFC curve that the presence of the peak of the blocking mechanism (T_B). It wants to define between the thermal energy and magnetic anisotropy energy of CCMO particles.(D. Mandal et al. 2019) It was noted that transition Temperature(Tc), the temperature at which maximum slope (dM/dT), recorded by the curve 180 K and blocking temperature (T_B) was 49 K where blocking temperature (Chen et al. 2016) is showing that under the blocking temperature the direction of solid in ZFC and FC is generally standing in exasperated interaction of ferromagnetic and antiferromagnetic in the magnetic system(Yadava et al. 2017a),('Possible incipient ferroelectricity in Mn-doped Na1/2Bi1/2Cu3Ti4O12: Applied Physics Letters: Vol 94, No 21' n.d.), ,(Verma et al. 2019).

Fig. (b) Indicates the magnetization versus magnetic field. It is indicated as M-H hysteresis loop,which is recorded as the temperature from 5 to 300 Kand resulting arisen that if the temperature gets decreases then trace and saturation magnetization increases,(D. Mandal et al. 2019) from this plotted graph, is recorded that coercivity was found to be 332 Oe , the saturation magnetization was observed to be approx ± 52 emu/g 5 to 300 K and reminding started value approx ± 60, which is above than theoretical value. (Kumar et al. 2019) This result also shows the confirm the purity of CCMO ceramic. (Latendresse et al. 2017) The squareness (Mr/Ms) of the ratio of CCMO ceramic in both temperature was found to be 0.87, from this result it is notified that the nature of CCMO ceramic has a hard crystal structure and permanent magnetic

and very valuable for soundtrack devices.(Yadava et al. 2017b) ,(Gonidec et al. 2011),(Verma et al. 2019)

It displays from Figure 3.11 (c) that the magnetic susceptibility of CCMO ceramic, In which temperature dependence magnetic susceptibility of indicating graph plot. This plot graph follow to Curie – Weiss low denoted by the following an equation

$$\frac{1}{\chi} = \frac{T}{C} - \frac{Tc}{C} \quad \text{.....(3)}$$

In represented equation (3) χ denoted as magnetic susceptibility, C denotes to Curie constant, Tc is denoted to Curie – Wiss law temperature and T denotes to Temperature in Kelvin. It is observed from the plot graph that we find out Curie content 54.54 emu g^{-1} Oe^{-1} and Curie - Weiss law 240 K above paramagnetic (PM). The positive value of Currie–Weiss temperature (Tc) highlight that the CCMO ceramics have ferromagnetic character. (Bhoi et al. 2013) It is observed from the plotted graph that in the transition temperature (disorder of Magnetic susceptibility) there is the formation of small cluster ferromagnetic domains in the paramagnetic region (PM) matrix the temperature range about 276 K to 222 K there is down term behavior in inverse magnetic susceptibility at 276 K which shows there is some form of small cluster of ferromagnetic domains in that region which is signature of Griffith's phase, it found to be an anomalous phase command within the PM region with an almost constant upper-temperature boundary. At this situation it more valuable for the concept of Griffith's who proposed a crystallographic disorder with the help of magnetic susceptibility in recent a few years ago, in which crystallographic disorder explained were found to be long-range ferromagnetic ordering temperature and this transition region temperature in the plotted graph ferromagnetic domains are dispersed in in the

paramagnetic matrix. This is known as intra-cluster magnetic ordering temperature through noticeable bulk Tc, which is varies depending on the size of the cluster, therefore lower to this spectrum of T_G known as Griffith's phase. It is denoted by symbol T_G .T_G also indicted in the graph Fig. 8 (C) by a purple colour arrow line and showing Griffith's temperature. (Thongbai et al. 2012),(Oner and Guler 2013),('Multiple magnetic transitions, Griffiths-like phase, and magnetoresistance in La2CrMnO6: Journal of Applied Physics: Vol 122, No 7' n.d.),(Thapa et al. n.d.),

It was found that the presence of such type of magnetic phase is mainly due to quenched disorder has been discovered through the linking of with giant magnetoresistance behavior of magnates non-Fermi liquid in d electron system is diluted to T_b–based intermetallic compound T_G is expected that it wants to prove the presence of favor Griffith's phase still is justified. (Deisenhofer et al. 2005),('Multiple magnetic transitions, Griffiths-like phase, and magnetoresistance in La2CrMnO6: Journal of Applied Physics: Vol 122, No 7' n.d.),

Figure 3.9 (C) showing a wonder features at the temperature range 222 K to 276 K signals of Griffith's phase region. It is known that the χ in the Griffiths phase is categorized by a supporter lower than unity.

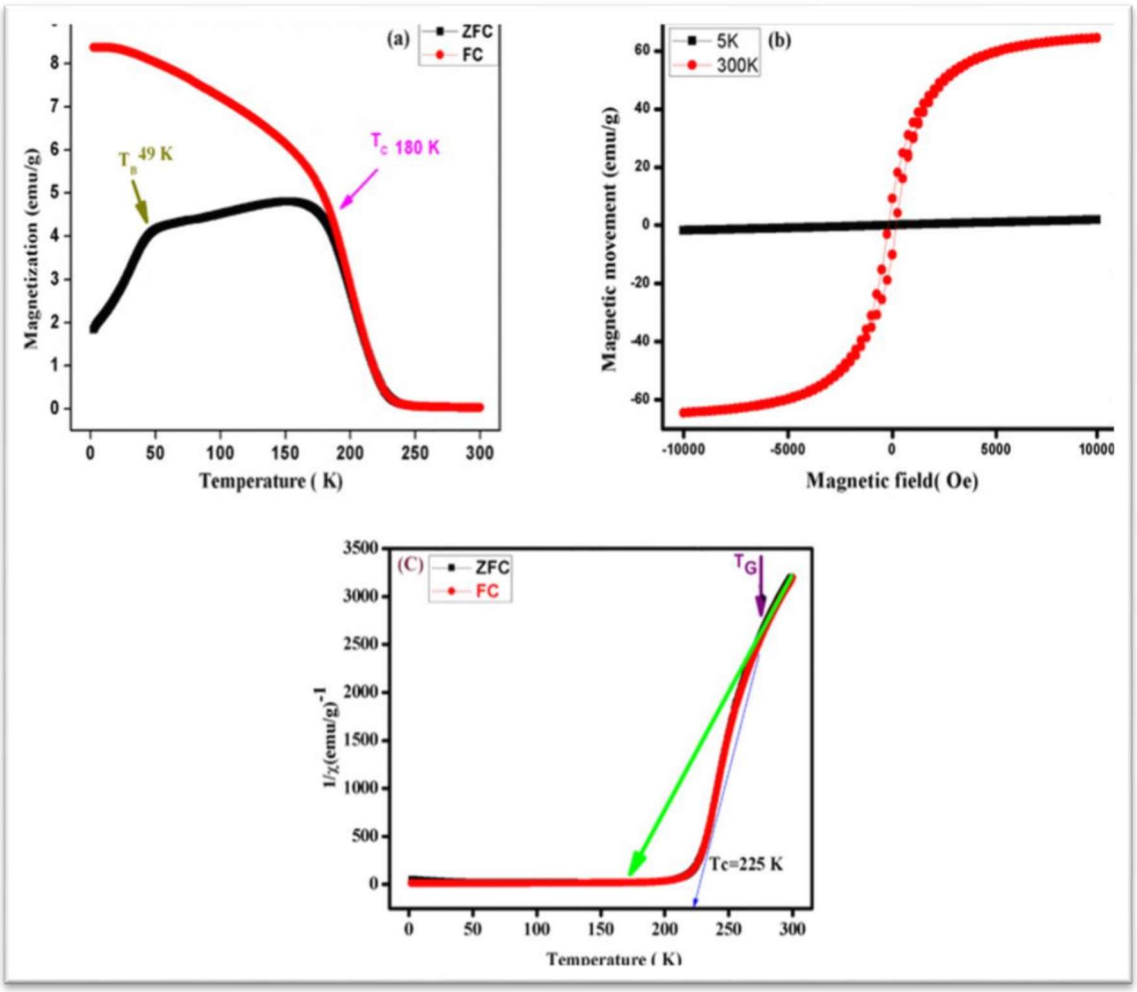

Figure 3.9. (a) Temperature dependence of ZFC and FC magnetization plot, top insert indicates dM /dT vs T **(b)** depicts the M-H hysteresis loop recorded at 5 and 300 k.

(C) Shows inverse magnetic susceptibility $1/\chi$ (T) for CCMO measured in the range of 0 to 300 K. The onset temperature T_G ,where $1/\chi$ (T) deviates from the linear temperature dependence (solid green line) are indicated by the arrows, showing the signature of Griffith's Phase behavior.

3.3.3. Dielectric studies

Figure 3.10 (a) and (b) display the variation of dielectric constant and tangent loss of CCMO ceramic with the temperature and few selected frequency, respectively. It was to be observed from the plotted the graph that the dielectric constant shows temperature-

independent 400 k to 500 k all measured frequency(100 Hz, 1 kHz,10 kHz, 100 kHz.It is observed from the plotted graph that the broad peak of dielectric constant was to be measured at around 423 k of all measured frequencies. It was to be observed that the dielectric constant decrease by increasing frequency.

Figure 3.10 (c) and (d) display that the dielectric constant and tangent loss against temperature of CCMO ceramic. The dielectric constant was to be recorded around 470,370, 260,150 at 100 Hz, 1 kHz, 10 KHz, and 100kHz at few selected frequencies. The broad peak of dielectric constant and dielectric loss of CCMO ceramic is due caused by oxygen vacancy created during the sintering process, not by the relaxation process.(Gautam et al. 2016b)The decreasing in the value of dielectric constant with frequency may be due to space charge polarisation.The oxygen vacancy during the sintering process is mainly due to the ceramic oxide material space charge polarization whose are mainly responds to external electric field. The charges have moved to longer distances in the materials at low frequency so that high dielectric constant observed, at high frequency the space charge polarization no longer follows so dielectric constant low.

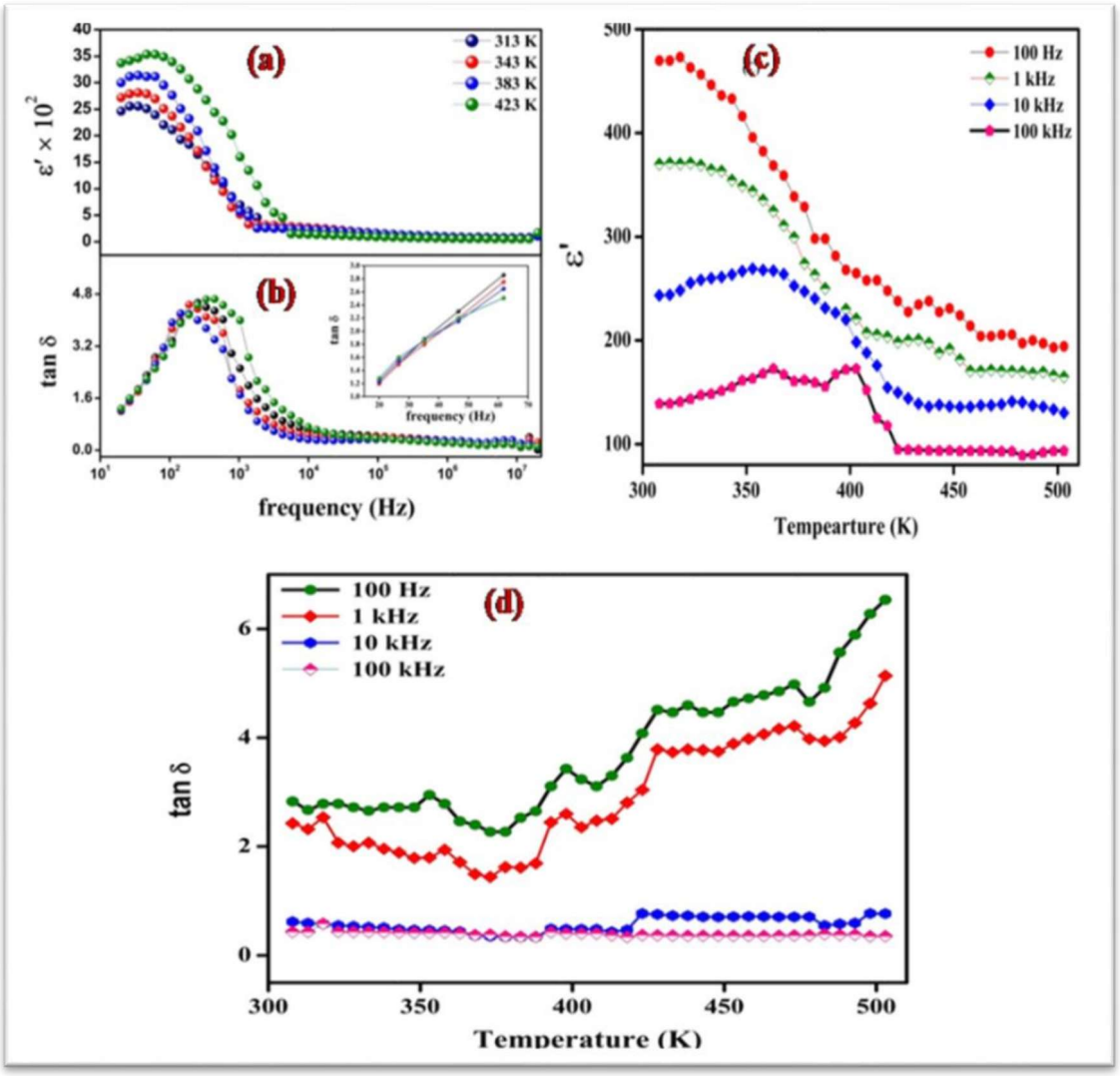

Figure 3.10. (a) and (**b)** display dielectric constant, the tangent loss against frequencies of CCMO ceramic, **(c)** and **(d)** tangent loss against temperature at few selected frequencies.

3.4. CONCLUSIONS

The $CaCu_3Mn_4O_{12}$ complex perovskite oxide ceramic was successfully synthesized through chemical method. The crystal phase formation of CCMO was confirmed by the XRD pattern 21 nm crystalline size. The thermal behavior was to be analyzed by thermogravimetric analysis (TGA) was found to that the phase formation of CCMO

ceramic was formed around 800℃ and microstructural studies was analysis through HR-TEM,FE-SEM,AFM particle was recorded in the range 100 to 200 nm, Morphology 6.6×10^2 nm range, Surface roughness around the range 30 to 40 nm. Chemical composition and Oxidation state recorded Calcium, Copper, Manganese, Oxygen was done by EDX and XPS spectra 5.15, 16.79, 22.97 and 55.06 atomic percentage and binding energy peak 347 eV and 350.6 eV, 934.54 eV and 954.23 eV, 641.4 eV and 652.4 eV, 929.7 eV and 931.6 eV respectively. Magnetic properties were studied with the existence of a wonderful Griffith's phase behavior in magnetic susceptibility disorder in CCMO ceramic. The transition was found to that there was form of some small cluster magnetic domains in the paramagnetic region (PM) matrix, temperature range about 276 to 222 K. There is down term behavior in inverse magnetic susceptibility at 276 k which shows there is some form of small cluster of ferromagnetic domains in that region which is signature of unique Griffith's phase (denoted by T_G). The value of dielectric constant and dielectric loss were found to be 3.3×10^2 and 1.2 at 10 Hz, respectively.

3.5 References

A. Molina-García, M., V. Rees, N., 2016. Effect of catalyst carbon supports on the oxygen reduction reaction in alkaline media: a comparative study. *RSC Advances* **6**, 94669–94681. https://doi.org/10.1039/C6RA18894J

Bhoi, D., Khan, N., Midya, A., Nandi, M., Hassen, A., Choudhury, P., Mandal, P., 2013. Formation of Nanosize Griffiths-like Clusters in Solid Solution of Ferromagnetic Manganite and Cobaltite. *J. Phys. Chem. C* **117**, 16658–16664. https://doi.org/10.1021/jp402726f

Chen, Y.-C., Liu, J.-L., Ungur, L., Liu, J., Li, Q.-W., Wang, L.-F., Ni, Z.-P., Chibotaru, L.F., Chen, X.-M., Tong, M.-L., 2016. Symmetry-Supported Magnetic Blocking at 20 K in Pentagonal Bipyramidal Dy(III) Single-Ion Magnets. *J. Am. Chem. Soc.* **138**, 2829–2837. https://doi.org/10.1021/jacs.5b13584

Chenavas, J., Joubert, J.C., Marezio, M., Bochu, B., 1975. The synthesis and crystal structure of CaCu3Mn4O12: A new ferromagnetic-perovskite-like compound. *Journal of Solid State Chemistry* **14**, 25–32. https://doi.org/10.1016/0022-4596(75)90358-8

D. Mandal, K., Kumar, A., Yadava, S., Singh, Dr.L., Kumar Verma, M., Singh, S., Kumar, V., 2019. Dielectric and electrical properties of zinc doped titanium oxide (TiO2) synthesized by semi-wet route. https://doi.org/10.1117/12.2518203

Deisenhofer, J., Braak, D., Krug von Nidda, H.-A., Hemberger, J., Eremina, R.M., Ivanshin, V.A., Balbashov, A.M., Jug, G., Loidl, A., Kimura, T., Tokura, Y., 2005. Observation of a Griffiths Phase in Paramagnetic La 1 − x Sr x MnO 3. *Phys. Rev. Lett.* **95**, 257202. https://doi.org/10.1103/PhysRevLett.95.257202

Gautam, P., Khare, A., Sharma, S., Singh, N.B., Mandal, K.D., 2016a. Characterization of Bi2/3Cu3Ti4O12 ceramics synthesized by semi-wet route. *Progress in Natural Science: Materials International* **26**, 567–571. https://doi.org/10.1016/j.pnsc.2016.11.008

Gautam, P., Khare, A., Sharma, S., Singh, N.B., Mandal, K.D., 2016b. Characterization of Bi2/3Cu3Ti4O12 ceramics synthesized by semi-wet route. *Progress in Natural Science: Materials International* **26**, 567–571. https://doi.org/10.1016/j.pnsc.2016.11.008

Gonidec, M., Biagi, R., Corradini, V., Moro, F., De Renzi, V., del Pennino, U., Summa, D., Muccioli, L., Zannoni, C., Amabilino, D.B., Veciana, J., 2011. Surface Supramolecular Organization of a Terbium(III) Double-Decker Complex on Graphite and its Single Molecule Magnet Behavior. *J. Am. Chem. Soc.* **133**, 6603–6612. https://doi.org/10.1021/ja109296c

Han, C.S., Choi, H.R., Choi, H.J., Cho, Y.S., 2017. Origin of Abnormal Dielectric Behavior and Chemical States in Amorphous $CaCu_3Ti_4O_{12}$ Thin Films on a Flexible

Polymer Substrate. *Chem. Mater.* **29**, 5915–5921. https://doi.org/10.1021/acs.chemmater.7b01346

Jaiswar, S., Mandal, K.D., 2017. Evidence of Enhanced Oxygen Vacancy Defects Inducing Ferromagnetism in Multiferroic CaMn $_7$ O $_{12}$ Manganite with Sintering Time. *J. Phys. Chem. C* **121**, 19586–19601. https://doi.org/10.1021/acs.jpcc.7b05415

Kim, C.H., Jang, Y.H., Seo, S.J., Song, C.H., Son, J.Y., Yang, Y.S., Cho, J.H., 2012. Effect of Mn doping on the temperature-dependent anomalous giant dielectric behavior of CaCu 3 Ti 4 O 12. *Phys. Rev. B* **85**, 245210. https://doi.org/10.1103/PhysRevB.85.245210

Kolev, N., Bontchev, R.P., Jacobson, A.J., Popov, V.N., Hadjiev, V.G., Litvinchuk, A.P., Iliev, M.N., 2002. Raman spectroscopy of ${\mathrm{CaCu}}_{3}{\mathrm{Ti}}_{4}{\mathrm{O}}_{12}$. *Phys. Rev. B* **66**, 132102. https://doi.org/10.1103/PhysRevB.66.132102

Kumar, A., Yadava, S.S., Gautam, P., Khare, A., Mandal, K.D., 2019. Magnetic and dielectric studies of barium hexaferrite (BaFe12O19) ceramic synthesized by chemical route. *J Electroceram* **42**, 47–56. https://doi.org/10.1007/s10832-018-0146-x

Latendresse, T.P., Bhuvanesh, N.S., Nippe, M., 2017. Hard Single-Molecule Magnet Behavior by a Linear Trinuclear Lanthanide–[1]Metallocenophane Complex. *J. Am. Chem. Soc.* **139**, 14877–14880. https://doi.org/10.1021/jacs.7b08690

Lin, J., Tong, P., Cui, D., Yang, C., Yang, J., Lin, S., Wang, B., Tong, W., Zhang, L., Zou, Y., Sun, Y., 2015. Unusual ferromagnetic critical behavior owing to short-range antiferromagnetic correlations in antiperovskite Cu1-xNMn3+x ($0.1 \leq x \leq 0.4$). *Sci Rep* **5**, 7933. https://doi.org/10.1038/srep07933

Lin, Y.-H., Cai, J., Li, M., Nan, C.-W., He, J., 2008. Grain boundary behavior in varistor-capacitor TiO2-rich CaCu3Ti4O12 ceramics. *Journal of Applied Physics* **103**, 074111. https://doi.org/10.1063/1.2902402

Liu, X., Fan, H., Shi, J., Dong, G., Li, Q., 2014. High oxide ion conducting solid electrolytes of bismuth and niobium co-substituted La2Mo2O9. *International Journal of Hydrogen Energy* **39**, 17819–17827. https://doi.org/10.1016/j.ijhydene.2014.08.110

Multiple magnetic transitions, Griffiths-like phase, and magnetoresistance in La2CrMnO6: Journal of Applied Physics: Vol 122, No 7 [WWW Document], n.d. URL https://aip.scitation.org/doi/10.1063/1.4999031 (accessed 8.21.19).

Nurulhuda, A., Warikh, A.R.M., Hafizzal, Y., 2017. Sol gel synthesis and characterization studies of Cupromanganite CaCu3Mn4O12. *IOP Conf. Ser.: Mater. Sci. Eng.* **226**, 012154. https://doi.org/10.1088/1757-899X/226/1/012154

Obrovac, M.N., Mao, O., Dahn, J.R., 1998. Structure and electrochemistry of LiMO2 (M=Ti, Mn, Fe, Co, Ni) prepared by mechanochemical synthesis. *Solid State Ionics* **112**, 9–19. https://doi.org/10.1016/S0167-2738(98)00225-2

de Oliveira, G.F., de Andrade, R.C., Trindade, M.A.G., Andrade, H.M.C., Teodoro de Carvalho, C., 2016. Thermogravimetric and spectroscopic study (TG–DTA/FT–IR) of activated carbon from the renewable biomass source Babassu. *Quim. Nova*. https://doi.org/10.21577/0100-4042.20160191

Oner, Y., Guler, A., 2013. Evidence of a Griffiths phase in a mixed compound of YFe2 and YFe3. *Journal of Applied Physics* **113**. https://doi.org/10.1063/1.4798623

Possible incipient ferroelectricity in Mn-doped Na1/2Bi1/2Cu3Ti4O12: Applied Physics Letters: Vol 94, No 21 [WWW Document], n.d. URL https://aip.scitation.org/doi/abs/10.1063/1.3134488 (accessed 8.21.19).

Sharma, S., Yadav, S.S., Singh, M.M., Mandal, K.D., 2014. Impedance spectroscopic and dielectric properties of nanosized $Y_{2/3}$ Cu_3 Ti_4 O_{12} ceramic. *J. Adv. Dielect.* **04**, 1450030. https://doi.org/10.1142/S2010135X14500301

Singh, L., Kim, I.W., Sin, B.C., Mandal, K.D., Rai, U.S., Ullah, A., Chung, H., Lee, Y., 2014. Dielectric studies of a nano-crystalline $CaCu_{2.90}$ $Zn_{0.10}$ Ti_4 O_{12} electro-ceramic by one pot glycine assisted synthesis from inexpensive TiO_2 for energy storage capacitors. *RSC Adv.* **4**, 52770–52784. https://doi.org/10.1039/C4RA08915D

Tang, W., Wu, X., Li, D., Wang, Z., Liu, G., Liu, H., Chen, Y., 2014. Oxalate route for promoting activity of manganese oxide catalysts in total VOCs' oxidation: effect of calcination temperature and preparation method. *Journal of Materials Chemistry A* **2**, 2544–2554. https://doi.org/10.1039/C3TA13847J

Tararam, R., Joanni, E., Savu, R., Bueno, P.R., Longo, E., Varela, J.A., 2011. Resistive-Switching Behavior in Polycrystalline $CaCu_3$ Ti_4 O_{12} Nanorods. *ACS Appl. Mater. Interfaces* **3**, 500–504. https://doi.org/10.1021/am101079g

Thapa, D.K., Islam, S., Saha, S.K., Mahapatra, P.S., Bhattacharyya, B., Sai, T.P., Mahadevu, R., Patil, S., Ghosh, A., Pandey, A., n.d. Coexistence of Diamagnetism and Vanishingly Small Electrical Resistance at Ambient Temperature and Pressure in Nanostructures 75.

Thongbai, P., Jumpatam, J., Putasaeng, B., Yamwong, T., Maensiri, S., 2012. The origin of giant dielectric relaxation and electrical responses of grains and grain boundaries of W-doped $CaCu_3$ Ti_4 O_{12} ceramics. *Journal of Applied Physics* **112**, 114115. https://doi.org/10.1063/1.4768468

Verde, M.G., Liu, H., Carroll, K.J., Baggetto, L., Veith, G.M., Meng, Y.S., 2014. Effect of Morphology and Manganese Valence on the Voltage Fade and Capacity Retention of

Li[Li2/12Ni3/12Mn7/12]O2. *ACS Appl. Mater. Interfaces* **6**, 18868–18877. https://doi.org/10.1021/am504701s

Verma, D.K., Kumar, B., Kavita, Rastogi, R.B., 2019. Zinc Oxide- and Magnesium-Doped Zinc Oxide-Decorated Nanocomposites of Reduced Graphene Oxide as Friction and Wear Modifiers. *ACS Appl. Mater. Interfaces* **11**, 2418–2430. https://doi.org/10.1021/acsami.8b20103

Yadava, S.S., Khare, A., Gautam, P., Kumar, A., Mandal, K.D., 2017a. Dielectric, ferroelectric and magnetic study of iron doped hexagonal Ba4YMn3O11.5−δ (BYMO) and its dependence on temperature as well as frequency. *New J. Chem.* **41**, 4611–4617. https://doi.org/10.1039/C6NJ04071C

Yadava, S.S., Khare, A., Gautam, P., Kumar, A., Mandal, K.D., 2017b. Dielectric, ferroelectric and magnetic study of iron doped hexagonal $Ba_4YMn_3O_{11.5-\delta}$ (BYMO) and its dependence on temperature as well as frequency. *New J. Chem.* **41**, 4611–4617. https://doi.org/10.1039/C6NJ04071C

Yamada, I., Takamatsu, A., Hayashi, N., Ikeno, H., 2017. Covalency Competition in the Quadruple Perovskite $CdCu_3Fe_4O_{12}$. *Inorg. Chem.* **56**, 9303–9310. https://doi.org/10.1021/acs.inorgchem.7b01405

Yang, Z., Lv, J., Pang, H., Yan, W., Qian, K., Guo, T., Guo, Z., 2015. Facile Synthesis of Coaxial CNTs/MnOx-Carbon Hybrid Nanofibers and Their Greatly Enhanced Lithium Storage Performance. *Sci Rep* **5**, 17473. https://doi.org/10.1038/srep17473

Zheng, Q., Fan, H., Long, C., 2012. Microstructures and electrical responses of pure and chromium-doped CaCu3Ti4O12 ceramics. *Journal of Alloys and Compounds* **511**, 90–94. https://doi.org/10.1016/j.jallcom.2011.09.002